Laboratory Experiments on Fault Shear Resistance Relevant to Coseismic Earthquake Slip

Report for SCEC Award #16026
Submitted April 28, 2017

Investigator: Terry E. Tullis, Brown University

I. Technical Report

A. SUMMARY

In the last few years we have turned our attention to laboratory experiments focused on understanding the widely discussed dynamic weakening mechanism termed *thermal pore-fluid pressurization,* hereafter abbreviated as TP. There are many theoretical and numerical studies of TP [*Andrews*, 2002; *Lachenbruch*, 1980; *Lee and Delaney*, 1987; *Mase and Smith*, 1985; 1987; *Noda*, 2008; *Noda and Shimamoto*, 2005; *Rempel and Rice*, 2006; *Rice*, 2006; *Rice and Cocco*, 2007; *Sibson*, 1973] and it is increasingly used in dynamic rupture and earthquake nucleation models [*Bizzarri and Cocco*, 2006a; b; *Lapusta and Rice*, 2004a; b; *Noda et al.*, 2009; *Noda and Lapusta*, 2010; *Rice et al.*, 2010; *Schmitt and Segall*, 2009; *Segall and Rice*, 2006]. Our experiment studies of thermal pressurization are the most definitive one yet obtained and we are nearly finished writing them up in a paper with David Goldsby as the first author.

With SCEC 2016 funding we have recently been conducting new experiments to further investigate fault-weakening via thermal pore-fluid pressurization, with an emphasis on trying to understand the role that fault-roughness-induced dilatancy may play in defeating this weakening mechanism on natural faults. We have heretofore demonstrated that thermal pressurization weakening occurs in our experiments on flat, but slightly roughened faults. However, both the theoretical and experimental results apply to flat surfaces, whereas natural faults have an approximately self-similar roughness, which is characterized by an amplitude-to-wavelength ratio of 10^{-3} to 10^{-2} in the slip direction [*Power and Tullis*, 1991; 1995; *Power et al.*, 1987; *Power et al.*, 1988]. Furthermore natural faults with this roughness are mated together across these surfaces [*Power and Tullis*, 1992]. This means that when faults slip, the roughness either becomes unmated or is accommodated by elastic and inelastic deformation. Accommodation, either by opening of the surfaces as would occur if the wall rocks were rigid, or by inelastic brittle deformation, or both, will result in dilatancy. Depending on the relative magnitude of the pore-volume increase and the volume increase of the thermally expanding pore fluid, the net effect on the pore pressure may either be a increase in pore pressure smaller than in the absence of dilatancy, or a reduction in pore pressure. In the latter case dilatancy hardening [*Lockner and Byerlee*, 1994] would occur rather than thermal pressurization weakening. All of the theoretical work on thermal pressurization weakening, as well as our continued experimental study of this process, will have no applicability to slip during earthquakes if a factor not included in those studies completely obliterates the weakening!

It is important to note that due to the approximately self-similar character of fault roughness, the dilatancy it produces will continue to become progressively larger as slip continues. This is because as more slip occurs the longer wavelength bumps that become unmated have higher amplitudes. Thus, this dilatancy is unlike a transient dilatancy due to a change in slip velocity that also occurs [*Beeler and Tullis*, 1997; *Lockner and Byerlee*, 1994; *Marone et al.*, 1990]. This transient dilatancy occurs at the onset of more rapid slip and is taken into account by the analysis of [*Rice*, 2006; *Segall and Rice*, 1995; 2006]. However, although *Rice* [2006] considers some effects that inelastic dilatancy may have on the properties of the near-fault material, none of the many theoretical and numerical studies of thermal pressurization weakening address the important issue of progressive dilatancy with continued slip.

The greatest dilatancy produced by sliding on initially mated rough surfaces of course occurs if all the accommodation occurs by normal opening. However, considerable dilatancy also occurs as a result of brittle failure and cataclastic flow. The particles produced by these processes do not fit together nearly as well as they did before the deformation occurred. Even though small particles can fit between larger ones, considerable void space is created between the fragments and this will produce suction on the pore fluid. How much dilatancy results from this process is unclear and remains to be determined by experiment.

Our previous rapid-sliding experiments were conducted on initially bare surfaces of Frederick Diabase that were thermally cracked [*Fredrich and Wong*, 1986] via temperature excursions in the range 725 ^{o}C to 806 ^{o}C, at a ramp rate of ~400 ^{o}C/hr. The resulting permeability depends on the treatment temperature. We realized last year that not only the fluid diffusivity of our samples but also their thermal diffusivity is changed somewhat by the thermal cracking. We have therefore been conducing experiments on un-heat-treated diabase that is essentially impermeable (10^{-23} m^2). We have tried an approach suggested to us by

Steve Hickman, namely to use an impermeable sample, roughen it somewhat to allow spaces for water to sit on the surfaces, and then pressurize them and let the trapped water build up pore pressure if it heats sufficiently.

In addition to changing to essentially impermeable samples, we have for the first time done experiments using both nominally flat surfaces as well as mated rough surfaces. We fabricated these mated rough surfaces by developing a new technique using a Computer Numerical Controlled (CNC) milling machine, as will be described below. Another change has involved a new way of roughening the surfaces at a small scale. In the past, because we have always used nominally flat surfaces that were prepared by grinding them flat with a surface grinder we could roughen them at a small scale using various sized grits on a glass plate. However, this method of producing small-scale roughness cannot be used on surfaces that are not nominally flat. Consequently we for the first time used sandblasting to roughen the rough-mated surfaces. Much of our effort this year was in developing these new techniques.

We have, however, also conducted experiments on both nominally flat and on mated rough surfaces at a normal stress of 100 MPa, about 4 times higher than our typical friction experiments. This was done in order that the stresses are higher so that deformation and comminution of the rock blocks are more likely to occur as they slide. The results of these preliminary experiments are presented here, even though the results of future experiments are likely to be more definitive once we refine our methods.

As a consequence of all of these changes we have learned a lot and are in a good position to obtain new results as we continue this work moving forward. The results presented herein are more focused on technical progress than scientific progress, although our results suggest that considerable deformation of the wall rocks does occur as mated rough surfaces slide.

B. REPORT

Figure 1 shows the topography (part A) that we have machined onto the mated surfaces in one of our experiments (338pfp) as well as the amplitude of the dilatant gap (part B) that would result as a function of slip if these initially mated samples were to behave rigidly. This upper-bound prediction of the amount

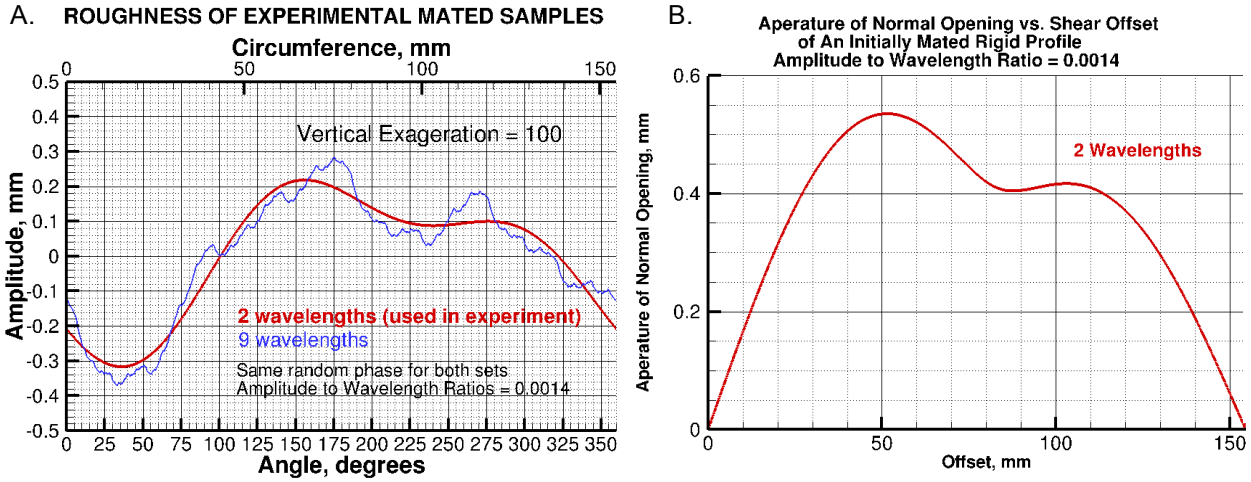

Figure 1. Plots in **A)** of the topography of the mated sample surfaces, and in **B)** of the gap that would result if they rotate relate to one another and move rigidly apart to accommodate each other's roughness. The red curve in **A)** is the topography that was specified via our CAD program (Solidworks) to the CNC milling machine. It was generated following the procedure described by *Power and Tullis* [1991], summing the topography from only two wavelenghs, the fundamental one and one with half that wavelength, their having random phase. This was used as a test of how the entire CNC milling process for preparing mated surfaces would work. The blue curve in **A)** shows how the topography would look if nine wavelengths were used. The curves are self-similar with an amplitude-to-wavelength ratio for all of them of 0.0014, a value that is in the range observed for natural faults of 0.001 to 0.01. For our trial of this entire method, we milled small plateaus (see Figure 3) with arc-lengths of 5 degrees. Note that this is the spacing of the finest marks on the grid in **A)** in the x direction of the plot. As figure 3 shows, we could mill smaller plateaus. Part **B)** shows the size of the gap that would result if mated samples with the red profile in **A)** is rotated and the rock accommodates the roughness only by rigidly riding up over the opposing face. Our results shown in Figure 5 suggest that the dilatancy is less than this. Whether the curve in **B)** is followed from the right or left end of the abscissa depends on in which sense the rotation occurs.

of dilatancy as a function of slip shown in Part B is compared with what we observed in experiment 338pfp in a later figure. Because it was a trial of many new techniques, this initial experiment involved mated topography that was generated by summing only two self-similar wavelengths, each of which had a realistic amplitude-to-wavelength ratio. Having shown that we are able successfully to machine realistic surface roughness into both halves of our sample so they mate initially, we are now in a position to machine surfaces with many more mated wavelengths, as shown in the blue curve of Figure 1A.

After the topography of Figure 1A is entered into a CAD model and those digital data are converted into CNC instructions, the machining can begin on each sample half. The process of physically creating the mated rough surfaces in the CNC is shown in Figure 2.

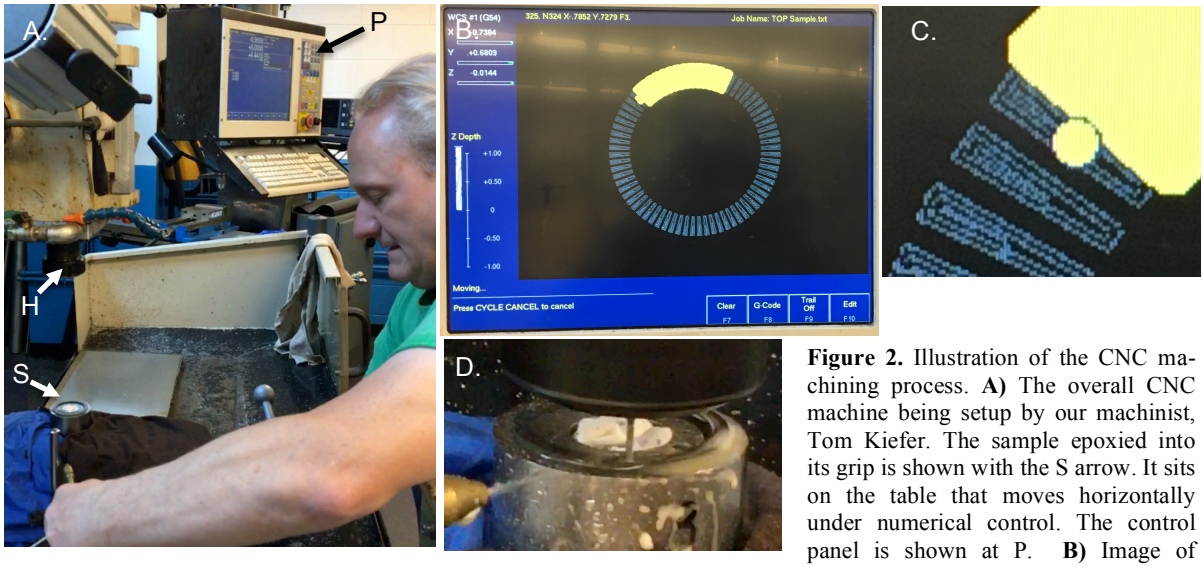

Figure 2. Illustration of the CNC machining process. **A)** The overall CNC machine being setup by our machinist, Tom Kiefer. The sample epoxied into its grip is shown with the S arrow. It sits on the table that moves horizontally under numerical control. The control panel is shown at P. **B)** Image of control screen showing in light blue the pattern to be machined and in yellow what has been finished. **C)** A detail of B, showing in blue the detailed track that will be followed by the program. A virtual image of the current end mill position is shown with the yellow dot. The wall thickness of our sample rings is 5 mm**. D)** A close up of the sample ring in its grip, the end mill shank, and the water-cooling nozzle. The cutter diameter of the head of the end mill is 2 mm.

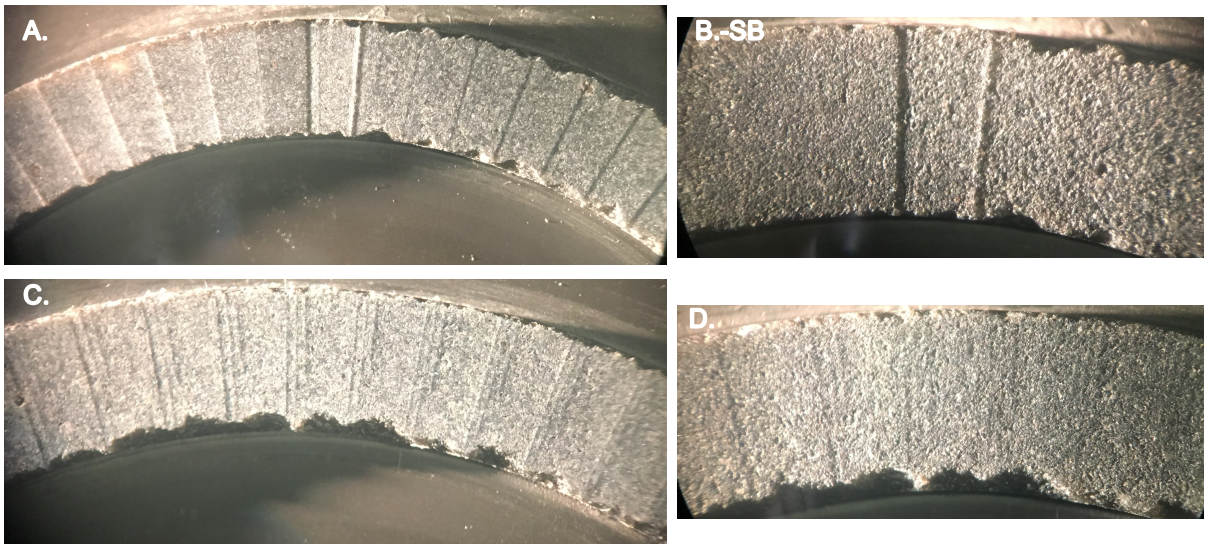

Figure 3. Photos of the surface of one of our two sample rings after CNC milling the surface to the required height. The 5 degree-wide pie-shaped plateaus seen in Figure 2C are visible. **A)** and **C)** are after milling, but prior to sandblasting. **B)** and **D)** are the same areas as in **A)** and **C)**, but after sandblasting and at a higher magnification. The wall thickness of our rings is 5 mm. **A)** and **B)** show the highest point around the circumference, whereas **C)** and **D)** show the lowest point. The sandblasting grains (currently 120 grit glass beads) need to be modified somewhat to allow greater roughening of the surface at a fine scale, both to remove the milling marks and to correspond better with the roughness typically used by roughening flat surfaces on a glass plate with 60 or 80 grit SiC.

The 5-degree-machined plateaus shown being created in Figure 2 are illustrated in Figure 3, both before and after sandblasting. The process creates mated surfaces as intended, but we need to use somewhat coarser grains in the sandblasting process. Side views of the surfaces, both in the mated and least-mated rotational orientations are shown in Figure 4 sitting on the bench prior to experiment 338pfp. The right hand-pair of photos (Figure 4B and 4D) show how well the faces are mated, while the left-hand pair (Figure 4 A and C) show the magnitude of the gap that would result if the sample halves were to behave rigidly as they rotate relative to one another.

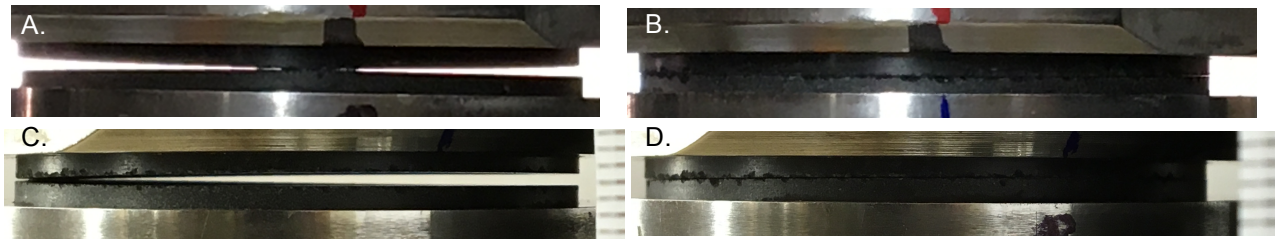

Figure 4. Visual illustration of the topography of the surfaces and how they do and do not fit together, depending on their relative orientation. A) and C) shows the surfaces with their high points each in contact, A) looking from the direction of the contacting high points, and C) looking at right angles to that., showing the largest gap that can form as the samples rotate if they do not deform. The tic-marks on the scale bars in C) and D) are mm, but they are somewhat in the foreground so the gap opening is slightly smaller than it appears. B) and D) are views from the same orientation relative to the sample grip with the A and B marked on them, but the other sample has been rotated so the two are perfectly mated. (Note that the area with the C and D labels is an inclined surface with a reflection that inadvertently makes it appear that there is no steel in that area.)

An overview of experiment 338pfp is shown in Figure 5. The measured dilatancy is smaller by a factor of

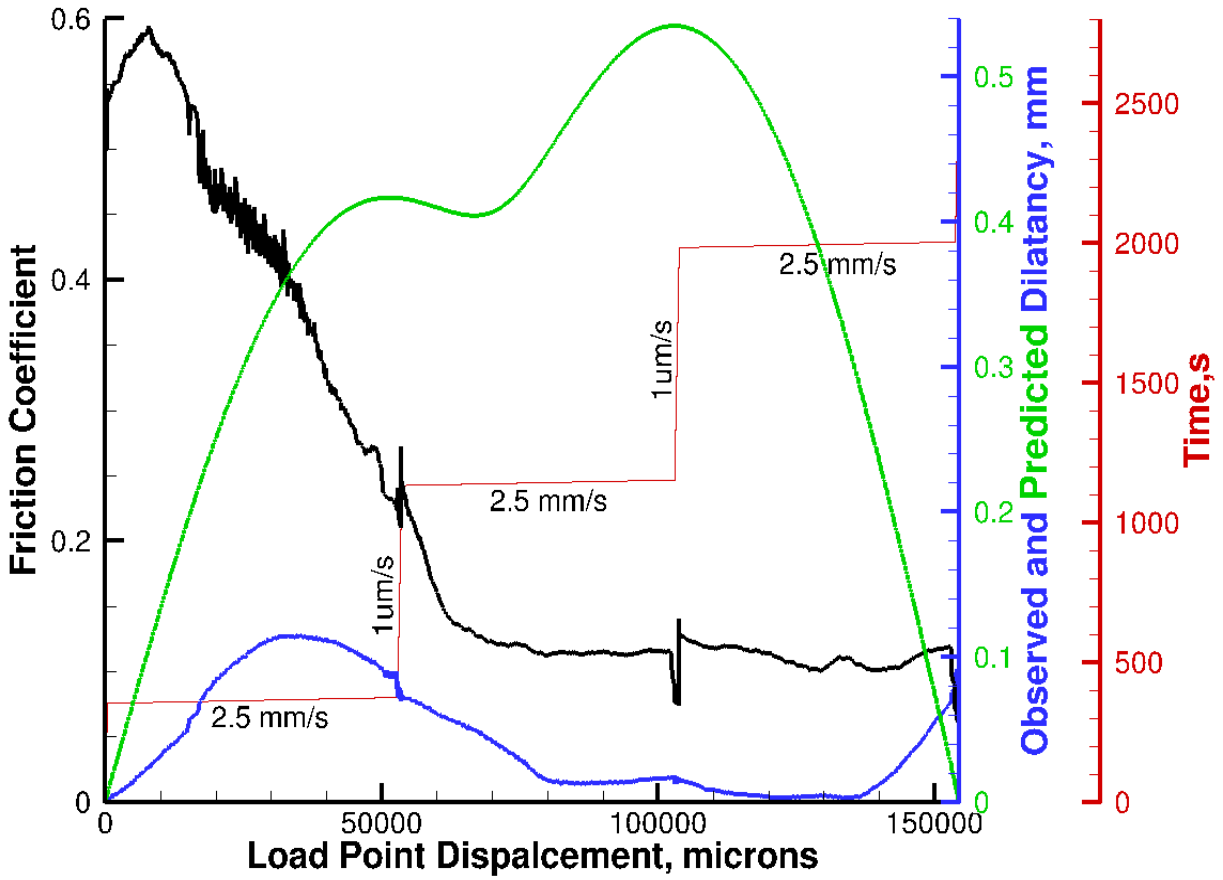

Figure 5. Results from experiment 338pfp, the preliminary experiment done on mated surfaces. The samples were slid 154.6 mm, one full revolution from their initial mated configuration. The observed dilation in blue is the downward movement of the lower piston by an external LVDT since the internal LVDT was off-scale. This is smaller than the predicted dilation for rigid samples in green (the curve of Figure 1B reversed due to sense of rotation used). The load-point displacement is based on the driving speed and elapsed time since neither slip-displacement transducer was working.

3-5 from that expected if the samples behaved rigidly, showing that permanent deformation occurred. Overall the net response was for the sample to dilate by about 80 microns which one would expect to have created very much more space than would be occupied by the water that was dripped onto the surfaces prior to the experiments if it underwent thermal expansion from shear heating. Three intervals of about 50 mm of slip at 2.5 mm/s were imposed between slow intervals when the velocity was only 1 micron/s. For reasons that are not at all clear, the friction fell nearly continuously during the experiment, although accompanying each increase in velocity, friction shows brief increases and then decreases (Figure 6). There is no clear evidence for thermal pressurization weakening, and none might be expected given the observed dilation. These results must be regardless as preliminary since several transducers were malfunctioning and the roughness created by the CNC milling machine was not designed to create the shorter wavelength roughness illustrated in blue in Figure 1. However, it appears that it is quite feasible to do experiments on samples with mated realistic roughness.

More details of the behavior during the high-speed sliding time intervals are shown in Figure 6.

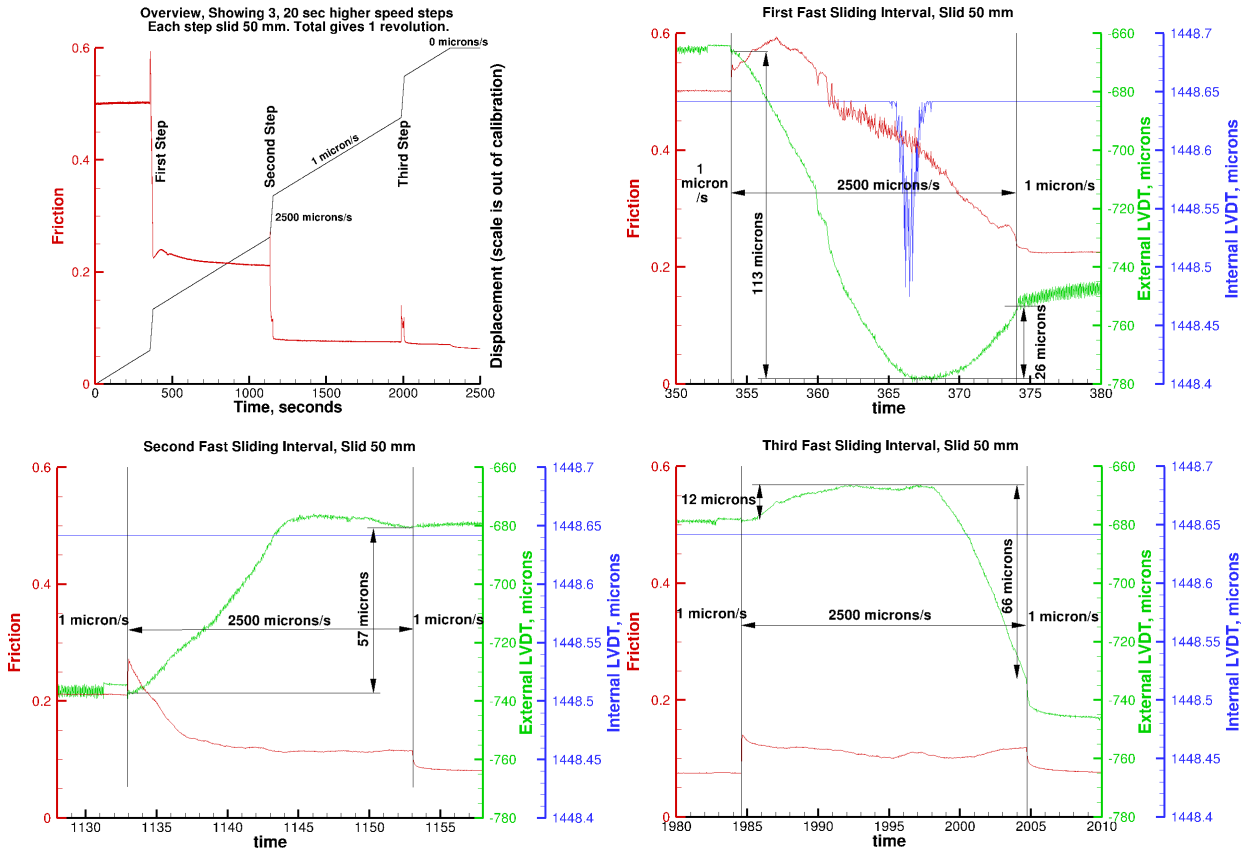

Figure 6. More details from experiment 338pfp. The upper left plot shows an overview of the results similar to Figure 5, but plotted time rather than slip. The other three show details of what occurred when the velocity was stepped from1 mm/s to 2500 mm/s three different times. Friction fell during the first two high-speed steps and the 1 mm/s loading-rate between higher-speed steps was too low for the stress to re-accumulate. Confining pressure is 98 MPa, and end-load from the hydraulic ram is 2 MPa, making normal stress equal to 100 MPa. Shear stress is therefore 100 times the plotted friction coefficient. Pore pressure is not measurable due to impermeable sample. However, confining-pressure gas cannot have leaked into the sample because if it had the friction would have dropped to 0.02 (=2 MPa/100 MPa). The observed weakening is not obviously due to thermal pressurization, although that is a possibility. Examination of the outer cylindrical surface of the sample after the experiment show some spalling of the edge, as might be expected from study of Figure 3. More detailed study of permanent deformation must await preparation of petrographic thin sections. Note that the internal LVDT which should be a better measure of the sample dilatancy was unfortunately configured so that it went off-scale during pressurization and so we have no record from it except of it's just peaking down from its off-scale limit in the first higher-speed segment (blue curve). However, we find that there is a good correlation between the signal from the internal and the external LVDTs, as observed in another experiment, so the data from the external LVDT should be good to within 10 mm or better, and hence this is what is plotted in blue in Figure 5.

C. REFERENCES CITED

Andrews, D. J. (2002), A fault constitutive relation accounting for thermal pressurization of pore fluid, *J. Geophys. Res.*, *107*, 12.

Beeler, N. M., and T. E. Tullis (1997), The roles of time and displacement in velocity-dependent volumetric strain of faults, *J. Geophys. Res.*, *102*, 22595-22609.

Bizzarri, A., and M. Cocco (2006a), A thermal pressurization model for the spontaneous dynamic rupture propagation on a three-dimensional fault: 1. Methodological approach, *J. Geophys. Res.*, *111*, B05303, doi:05310.01029/02005JB003862.

Bizzarri, A., and M. Cocco (2006b), A thermal pressurization model for the spontaneous dynamic rupture propagation on a three-dimensional fault: 2. Traction evolution and dynamic parameters, *J. Geophys. Res.*, *111*, B05304, doi:05310.01029/02005JB003864.

Fredrich, J. T., and T.-f. Wong (1986), Micromechanics of thermally induced cracking in three crustal rocks, *J. Geophys. Res.*, *91*, 12,743-712,764.

Lachenbruch, A. H. (1980), Frictional heating, fluid pressure, and the resistance to fault motion, *J. Geophys. Res.*, *85*, 6249-6272.

Lapusta, N., and J. R. Rice (2004a), Earthquake sequences on rate and state faults with strong dynamic weakening, *Eos. Trans. Am. Geophys. Union, Fall Meeting Suppl.*, *85*(47), T22A-05.

Lapusta, N., and J. R. Rice (2004b), Earthquake sequences on rate and state faults with strong dynamic weakening, paper presented at 2004 SCEC Annual Meeting Proceedings and Abstracts, Southern California Earthquake Center, PalmSprings, California, 2004.

Lee, T. C., and P. T. Delaney (1987), Frictional Heating and Pore Pressure Rise Due to a Fault Slip, *Geophysical Journal of the Royal Astronomical Society*, *88*(3), 569-591.

Lockner, D. A., and J. D. Byerlee (1994), Dilatancy in hydraulically isolated fault and the suppression of instability, *Geophys. Res. Lett.*, *21*, 2353-2356.

Marone, C. J., C. B. Raleigh, and C. H. Scholz (1990), Frictional behavior and constitutive modeling of simulated fault gouge, *J. Geophys. Res.*, *95*, 7007-7025.

Mase, C. W., and L. Smith (1985), Pore-fluid pressures and frictional heating on a fault surface, *Pure Appl. Geophys.*, *122*, 583-607.

Mase, C. W., and L. Smith (1987), Effects of frictional heating on the thermal hydrologic and mechanical response of a fault, *J. Geophys. Res.*, *92*, 6249-6272.

Noda, H. (2008), Frictional constitutive law at intermediate slip rates accounting for flash heating and thermally activated slip process, *J. Geophys. Res.*, doi:10.1029/2007JB005406.

Noda, H., E. M. Dunham, and J. R. Rice (2009), Earthquake ruptures with thermal weakening and the operation of major faults at low overall stress levels, *J. Geophys. Res.*, *114 (B07302)*, doi:10.1029/2008JB006143.

Noda, H., and N. Lapusta (2010), Three-dimensional earthquake sequence simulations with evolving temperature and pore pressure due to shear heating: Effect of heterogeneous hydraulic diffusivity, *J. Geophys. Res.*, *115*, B12314.

Noda, H., and T. Shimamoto (2005), Thermal pressurization and slip-weakening distance of a fault: An example of the Hanaore fault, southwest Japan, *Bull. Seis. Soc. Am.*, *95*(4), 1224-1233.

Power, W. L., and T. E. Tullis (1991), Euclidian and fractal models for the description of rock surface roughness, *J. Geophys. Res*, *96*, 415-424.

Power, W. L., and T. E. Tullis (1992), The contact between opposing fault surfaces at Dixie Valley, Nevada, and implications for fault mechanics, *J. Geophys. Res.*, *97*, 15425-15435.

Power, W. L., and T. E. Tullis (1995), A review of the fractal character of natural fault surfaces with implications for friction and the evolution of fault zones, in *Fractals in The Earth Sciences*, edited by P. Lapointe and C. Barton, pp. 89-105, Plenum, New York.

Power, W. L., T. E. Tullis, S. R. Brown, G. N. Boitnott, and C. H. Scholz (1987), Roughness of natural fault surfaces, *Geophys. Res. Lett*, *14*, 29-32.

Power, W. L., T. E. Tullis, and J. D. Weeks (1988), Roughness and wear during brittle faulting, *Jour. Geophys. Res*, *93*(B12), 15,268-215,278.

Rempel, A. W., and J. R. Rice (2006), Thermal pressurization and onset of melting in fault zones, *Journal of Geophysical Research-Solid Earth*, *111*(B9), B09314, doi:09310.01029/02006JB004314.

Rice, J. R. (2006), Heating and weakening of faults during earthquake slip, *Journal of Geophysical Research-Solid Earth*, *111*(B5), doi:10.1029/2005JB004006.

Rice, J. R., and M. Cocco (2007), Seismic fault rheology and earthquake dynamics, in *The Dynamics of Fault Zones*, edited by M. R. Handy, p. in press, MIT Press, Cambridge, Mass.

Rice, J. R., E. M. Dunham, and H. Noda (2010), Thermo- and hydro-mechanical processes along faults during rapid slip, in *Meso-Scale Shear Physics in Earthquake and Landslide Mechanics*, edited by Y. Hatzor, J. Sulem and I. Vardoulakis, pp. 3-16, CRC Press.

Schmitt, S. V., and P. Segall (2009), Thermal pressurization during “slip law” frictional earthquake nucleation, *Poster, 2009 SCEC Annual Meeting*.

Segall, P., and J. R. Rice (1995), Dilatancy, compaction, and slip instability of a fluid infiltrated fault, *J. Geophys. Res.*, *100*, 22155-22173.

Segall, P., and J. R. Rice (2006), Does shear heating of pore fluid contribute to earthquake nucleation?, *Journal of Geophysical Research-Solid Earth*, *111 (B09316)*, doi:10.1029/2005JB004129.

Sibson, R. H. (1973), Interactions between temperature and fluid pressure during earthquake faulting - A mechanism for partial or total stress relief, *Nature*, *243*, 66-68.